Journal of Neuroscience Methods 134 (2004) 101–107

JOURNAL OF NEUROSCIENCE METHODS

www.elsevier.com/locate/jneumeth

Double labeling serial sections to enhance three-dimensional imaging of injured spinal cord

Bradley S. Duerstock*

Department of Basic Medical Sciences, Center for Paralysis Research, Institute for Applied Neurology, School of Veterinary Medicine, Purdue University, 408 South University Street, West Lafayette, IN 47907, USA

Received 5 September 2003; received in revised form 16 October 2003; accepted 21 November 2003

Abstract

A method of double labeling a set of serial histological sections was performed to produce multiple three-dimensional (3D) reconstructions from the same segment of injured spinal cord. Alternate groups of consecutive histological sections were stained with Luxol fast blue with cresyl violet and Mallory's trichrome in order to reconstruct two different 3D images that reveal different pathological features of the same 1-month-old compression spinal cord injury. Three-dimensional visualization of the two reconstructions was accomplished using an isocontouring algorithm that automatically extracts surfaces of features of interest based on pixel intensity. The two 3D reconstructions demonstrated the sparing of myelinated nerve fibers and the composition of neuroglia through the chronic lesion of an adult guinea pig. The 3D images provided a comprehensive and explicit view of a chronically injured spinal cord that is not possible by the inspection of two-dimensional (2D) histological sections or from magnetic resonance imaging. Using every histological section, we believe this double labeling 3D reconstruction technique provides a more enhanced and accurate visualization of the entire spinal cord lesion than has been possible before. Furthermore, we contend that this double labeling technique can further elucidate the histopathological events of secondary injury at different time points post-injury by using different combinations of complementary histological makers.
© 2003 Elsevier B.V. All rights reserved.

Keywords: Three-dimensional reconstruction; 3D imaging; 3D visualization; Spinal cord injury; Neurotrauma; Histopathology

1. Introduction

Due to advances in technology the use of three-dimensional (3D) reconstruction from serial sections has increased. The source of sections for 3D reconstruction range from histology to computed tomography (CT) to magnetic resonance imaging (MRI). 3D reconstruction is ideal for imaging the morphology of internal anatomical structures. In neuroscience this has included; obscured regions of the brain (Halliday et al., 1993; Roesch et al., 1996), inner ear (Chimento et al., 1994; Hashimoto and Kimura, 1988), and the developing nervous system (Hounnou et al., 2003). In the field of neurotrauma, 3D reconstruction has been used to image the occult damage occurring in the central grey and white matter after contusion and compression injuries to the mammalian spinal cord (Beattie et al., 1997; Bresnahan et al., 1991; Duerstock and Borgens, 2002; Duerstock et al., 2000).

When evaluating a complicated structure, like a damaged spinal cord, 3D reconstruction permits a more comprehensive and detailed view of the lesion than by evaluating a sample of histological sections from the epicenter of the injury site (Balentine, 1978; Moriarty et al., 1998). The isocontouring software we use allows us to reconstruct three-dimensional surfaces around features of interest, which can be measured for volume and surface area. 3D surfaces are automatically rendered when the threshold of an anatomical feature is selected. Thus, no matter how complicated the histological structure(s), it can be easily imaged and measured (Duerstock et al., 2000). In the past, 3D surface reconstructions have been successfully used to compare the 3D shape and size of injury sites between blinded experimental and control groups of injured spinal cord (Duerstock and Borgens, 2002). 3D reconstruction can image pathological changes throughout the entire spinal cord lesion. This is especially useful in instances where amelioration of behavior is observed but anatomical changes are subtle. 3D reconstruction reveals images of the complete lesion with the perception of depth and substance.

* Tel.: +1-765-494-7600; fax: +1-765-494-7605.
E-mail address: bsd@purdue.edu (B.S. Duerstock).

0165-0270/$ – see front matter © 2003 Elsevier B.V. All rights reserved.
doi:10.1016/j.jneumeth.2003.11.012

Two-dimensional (2D) histological sections cannot achieve this.

3D reconstructions from histological sections are able to discriminate and label vastly more anatomical features of interest than with MRI or CT scans because of the large availability of specific tissue stains and immunohistochemical markers. This is particularly useful when evaluating different necrotic cascades that occur during secondary injury of the spinal cord. Secondary injury occurs after the initial trauma to the spinal cord and is characterized by a profound inflammatory reaction, gliosis, cavitation, and the progressive dissolution of nerve fibers (Tator and Fehlings, 1991; Young et al., 1995). Understanding the timing and peaks of these events and the cell types involved is difficult to track. Multiple stains applied to histological sections can label a number of different pathological processes occurring during secondary injury.

We have extended the capability to image histopathology by employing a double labeling technique that produces multiple 3D reconstructions from the same histological data set with little user intervention. By using two different histological stains to label alternate groups of serial tissue sections we were able to surface reconstruct a greater number of pathological features for a single injured segment of spinal cord. We believe that this new technique of producing double-labeled 3D reconstructions allows us to image the injured spinal cord: (1) more comprehensively than from 2D histological sections; and (2) with greater selectivity and accuracy than from previous 3D reconstruction methods. This has significant usage in the study of spinal cord injury where multiple necrotic and inflammatory events occur simultaneously.

2. Materials and methods

2.1. Animals

An adult (300 g) laboratory guinea pig was used in this experiment. The animal was euthanized 1 month post-treatment by anesthesia with 0.2 ml of ketamine·HCl and 0.2 ml of xylazine then an overdose of sodium pentobarbital (0.8 ml of 1 g/ml standard injectable) immediately followed by perfusion/fixation with 6% paraformaldehyde, 0.5% glutaraldehyde in a phosphate buffer. The spinal cord was dissected free and immersion fixed in the above fixative for approximately 18 h.

2.2. Surgical procedures

Anesthesia was performed using an intra-muscular injection of 0.1 ml/100 g body weight of a standardized solution of 100 mg/kg of ketamine·HCl and 20 mg/kg of xylazine. The spinal cord was exposed by a partial laminectomy (11th to 12th thoracic vertebrae; dura left intact) and the dorsal hemisphere compressed for 15 s using blunted Watchmakers' forceps with a detente to standardize displacement of the spinal cord. The incisions were closed in layers with 3–0 proline suture and the skin closed with wound clips. Immediately the post-surgery, the animal was subcutaneously injected with 3 ml lactated ringers to prevent dehydration, and the animal placed under a heat lamp for about 24 h to reduce post-surgical mortality due to shock.

2.3. Histological preparation

The spinal cord segment containing the compression injury site was dehydrated in ascending concentrations of alcohol followed by xylene permitting infiltration and embedded in paraffin. The segment of spinal cord 3–4 mm long was transversely sectioned at 15 μm. Ten consecutive sections were mounted on a slide. Paraffin was removed by 1 h treatment in a 60 °C oven followed by a 1 h immersion in 100% xylene. Sections were rehydrated by immersions in descending grades of alcohol to distilled water by conventional methods (Duerstock and Borgens, 2002). Every other slide was stained with either Mallory's trichrome (MT) or Luxol fast blue (LFB) counterstained with cresyl violet, rinsed, and coverslipped in permount.

2.4. Video capturing and registration of sections for 3D visualization

A color video camera (Optronics DEI-750, Goleta, CA) attached to the Olympus Van Ox Universal (Optical Analysis, Indianapolis, IN) microscope captured histological sections on a Intel® personal computer using Adobe Photoshop® software. Registration was performed by aligning each histological section to be captured to the previous histological image. Anatomical features served as fiducial markers (Duerstock et al., 2000). The set of histological images were managed and three-dimensionally reconstructed on a Silicon Graphics® Indigo computer (Mountain View, CA).

2.5. Three-dimensional reconstruction

The segment of spinal cord was three-dimensionally reconstructed from a set of 226 transverse sections using an isocontouring software program (Bajaj et al., 1997). The isocontouring algorithm automatically extracts and reconstructs three-dimensional polygonal contours around features of interest based on common isovalues of the component sections. The display of isocontours of interest was determined from a spectrum interface. A filter was used to reduce noise inherent to the histological sections. The isocontouring filter employed both convolution and averaging steps. Convolution reduced noise in each histological image by normalizing the pixel values within each section. Throughout each spinal cord data set, consecutive overlapping groups of three adjacent sections were averaged together to diminish any artifacts or histological defects present in a section. Averaging

allowed only biological features that were consistent in two or more sections to be three-dimensionally reconstructed, thus eliminating any outlier histological defects from the 3D image (Duerstock et al., 2000).

Every consecutive section was used to three-dimensionally reconstruct a full or complete 3D image. We also produced a separate 3D reconstruction from half the sections that was stained with Mallory's trichrome and another 3D reconstruction was generated from Luxol fast blue and cresyl violet staining. In order to three-dimensionally reconstruct each half of the data set, we replaced the alternate groups of ten sections that were missing by copying them from the end sections bordering that group to maintain the original number of sections. This produced 3D images in which 50% of the data set was interpolated.

3. Results

Fig. 1 shows histological sections at the distal ends and lesion epicenter from the same spinal cord segment. In Fig. 1A and B sections stained with Mallory's trichrome (MT) was used to define the chronic 1-month-old spinal cord injury. The section in Fig. 1A is distal from the injury site. Nuclei of the grey matter were labeled bright red. Neuroglial staining was also prevalent in the white matter evidenced by dark red coloration. The beginning of the cavitated lesion could be seen at the most dorsal aspect of the ventral columns (Fig. 1A). Fig. 1B shows a section from the injury epicenter where the severity of the compression destroyed most of the dorsal hemisphere. Cavitation and disorganized tissue is found throughout the remaining parenchyma. The

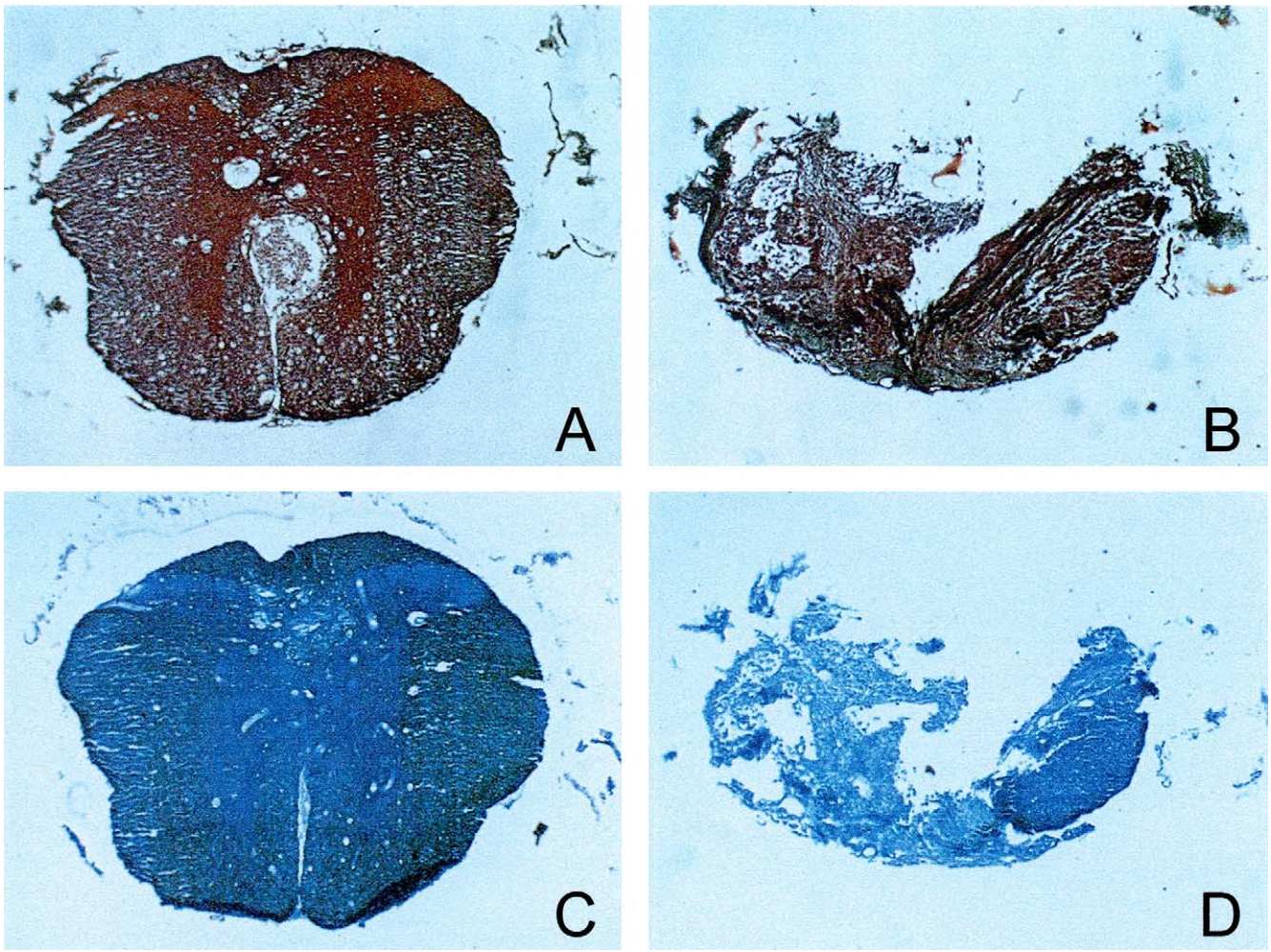

Fig. 1. Sample histological sections used in the double-labeled 3D reconstruction. All micrographs show 15 μm-thick transverse sections with the dorsal surface toward the top of the page. (A) A transverse section labeled with Mallory's trichrome is from the distal end of the spinal cord segment. The neurons of the grey matter stained bright red and the nuclei of the glia in the surrounding white matter appeared dark red. Cavitation from the lesion can be seen at the dorsal portion of the ventral columns. (B) Transverse section from the epicenter of the injury site stained with MT. The compression injury caused the section to be deformed into an elliptical shape with profound loss of tissue in the dorsal hemisphere. The only dark red staining occurred at the ventral rim of white matter. Higher magnification showed cavitation, gliosis, and collagen-like deposition at the center and dorsal regions of the spinal cord. (C) An alternate transverse section taken from the same distal end of the spinal segment as in (A) labeled with Luxol fast blue and counterstained with cresyl violet. The myelinated white matter tracts appeared dark blue and the grey matter is bright blue. (D) A LFB cross-section from the lesion epicenter. As in (B) most of the dorsal tissue is lost. Sparing of myelinated nerve fibers can be seen at the right ventrolateral tracts shown in dark blue.

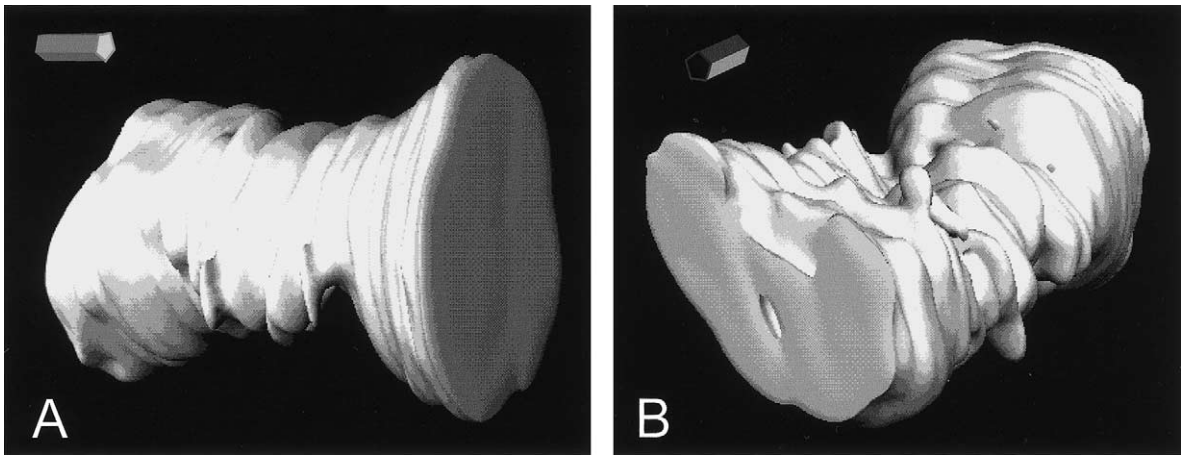

Fig. 2. 3D reconstruction from the complete set of spinal cord histological sections. These reconstructions were produced using every consecutive section in a segment of spinal cord approximately 3.5 cm long. The orientation icon illustrates the orientation of the 3D reconstruction of the spinal cord segment in each subsequent figure. The black end of the pentagonal cylinder indicates the caudal end of the spinal segment. The white end indicates the rostral end of the segment. The surface of the pentagonal cylinder that forms the vertex represents the dorsal surface of the spinal cord and the base of the pentagonal icon refers to the ventral surface. In (A), the 3D reconstruction of the spinal segment is oriented horizontally to reveal the hour-glass shape after compression. The sections at the distal ends of the reconstruction are mostly undamaged. (B) shows dissolution of nervous tissue in the dorsal hemisphere. Most significant tissue loss occurred at the site of compression.

only organized nervous tissue existed at the ventral rim of the spinal cord (Fig. 1B).

In Fig. 1C and D histological sections labeled with Luxol fast blue (LFB) and a cresyl violet counterstain revealed myelinated axons and cell bodies. The dark blue staining of myelinated spinal cord tissue with LFB was apparent in histological slices and subsequent 3D reconstructions (Fig. 1C). Cresyl violet allowed the nuclei of the grey matter to be seen. Fig. 1D shows a histological section from the lesion epicenter. Intact myelinated nervous tissue stained dark blue could only be observed at the right ventrolateral subpial rim of the spinal cord. Most nervous tissue either deteriorated or became cavitated (Fig. 1D). 3D reconstructions from these sections extrapolated these two-dimensional pathological features into a more comprehensive view of the overall lesion of the chronically injured spinal cord.

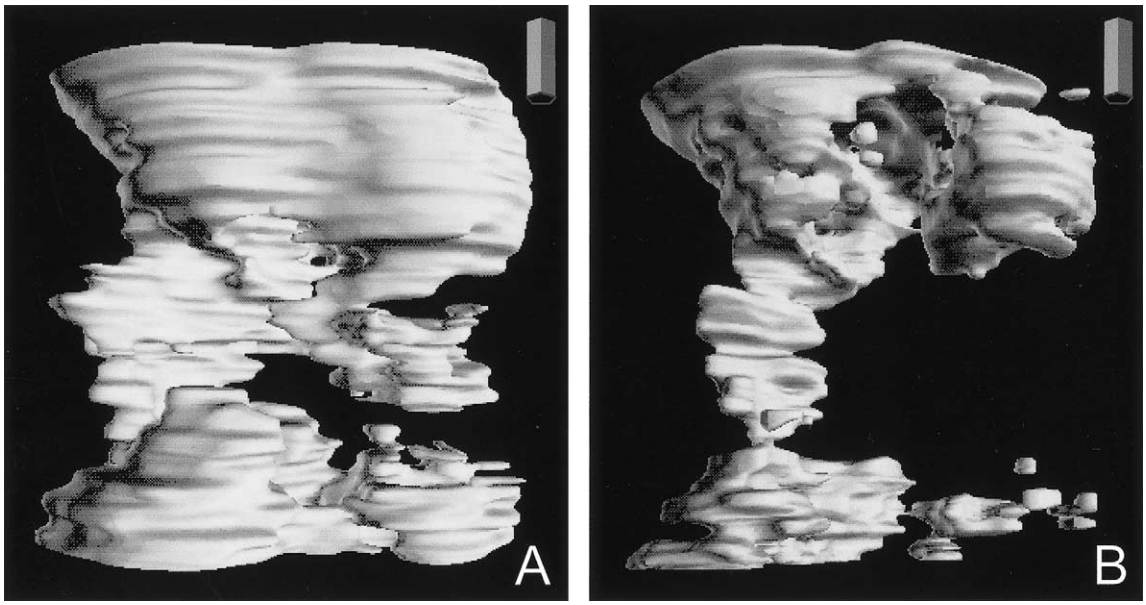

Fig. 3. 3D reconstructions from MT and LFB sets of histological sections. (A) Dorsal view of the 3D reconstruction produced from MT stained sections. Spaces produced from the absence of LFB sections were interpolated from bordering MT sections. This reconstruction visualizes the presence of glia and neuronal cell bodies in the spinal cord injury. Robust labeling was discerned at the distal ends of the spinal segment and at the ventral white matter tracts at the injury site. (B) Dorsal view of the 3D reconstructed LFB stained sections. Labeled myelinated fibers were found at the uninjured ends of the spinal segment and sparsely found at the ventral subpial rim of white matter at the lesion site.

Fig. 2 shows the injured spinal cord segment three-dimensionally reconstructed using every serial section from the combined sets of MT and LFB stained sections. The site of compression was evident by the hourglass shape of the spinal cord where the center was severely compressed while the rostral and caudal ends of the segment are intact. The compressed and absent nervous tissue parenchyma in the dorsal hemisphere of the spinal cord at the injury site could be discerned from the full 3D reconstruction (Fig. 2B).

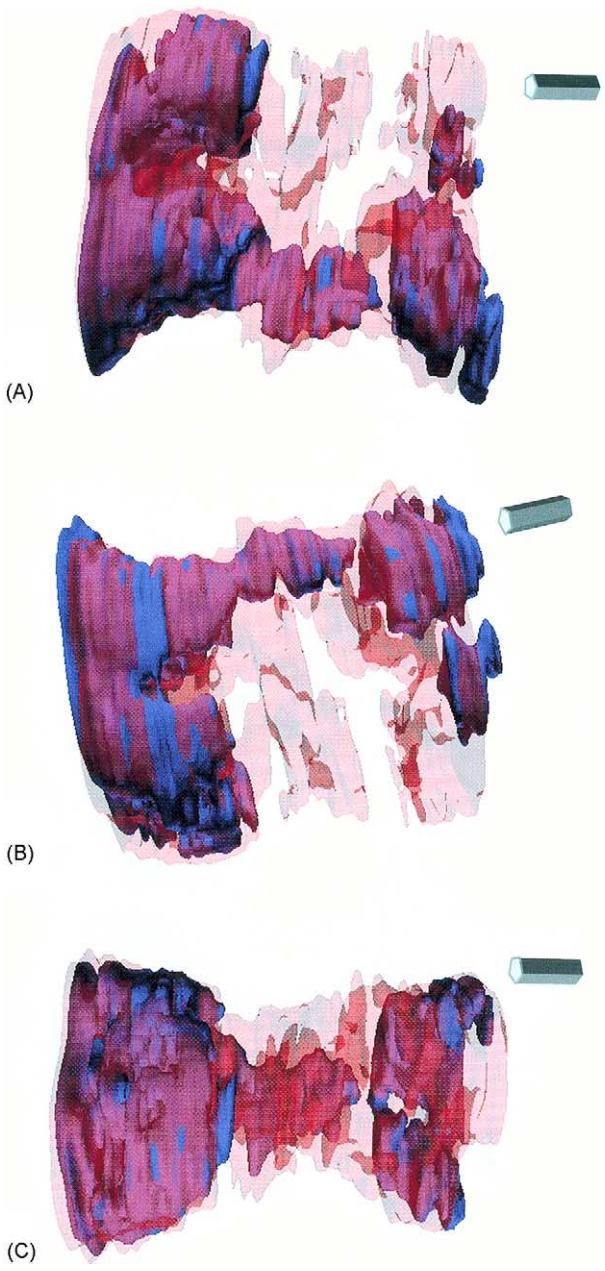

Fig. 4. Combination of MT and LFB 3D reconstructions. The MT 3D reconstruction shown in red is transparent to better reveal the blue 3D reconstruction of LFB stained sections. The combined 3D images each with the caudal end of the spinal segment on the left-hand side are rotated vertically: (A) dorsal view; (B) ventral view; and (C) lateral view with the dorsal surface toward the bottom of the page. The LFB reconstruction is more selective labeling only myelinated nerve fibers. The larger MT reconstruction demonstrates the lingering presence of nucleated cells through the lesion. These combined 3D reconstructions illustrate this chronic lesion as nearly devoid of myelinated nerve fibers but not particularly favorable for MT stained cells either.

By interpolation the MT and LFB groups of sections were separated to produce two distinct 3D reconstructions. Fig. 3A shows a 3D reconstruction from MT stained sections. This reconstruction demonstrates the extent of cavitation and amount of darkly stained neuroglia and grey matter. The nervous tissue at the distal ends of the spinal segment, rostral and caudal to the injury site, was mostly intact. Fig. 3B images the portions of the spinal cord segment stained with LFB. This 3D reconstruction shows the viable myelinated parenchyma. Darkly labeled myelin was observed at the ends of the spinal cord and partially at the ventral subpial rim of the injury site. Typical for a compression injury most damage occurred in the central grey and white matter with sparing of tracts at the perimeter of the spinal cord (Blight, 1991).

Evident in Fig. 3A and B, there was a large overlap of MT and LFB stained tissue. By overlaying these two reconstructions the differences in labeled tissue can be seen (Fig. 4). The two reconstructions corresponded quite closely at the distal ends of the spinal cord segment, which consisted mostly of intact, myelinated neural tissue, and at portions of myelinated white matter at the ventral rim of the injury site (Fig. 4B). Less spinal cord parenchyma was visualized with LFB than with MT because of higher selectivity of LFB for labeling only myelinated neurons. The comparison of MT and LFB reconstructions shows that there is variable staining of neuronal and glial nuclei through the lesion but myelinated fibers were sparse.

In Fig. 5, each specific labeled 3D reconstruction was compared to the full 3D reconstruction consisting of both MT and LFB sets of sections. In Fig. 5A and B, the MT reconstruction was overlaid with the full MT-LFB 3D reconstruction. Due to the ubiquitous staining of nervous tissue by MT, both reconstructions corresponded closely. In Fig. 5C and D, the more specific LFB reconstruction was merged with the full MT-LFB reconstruction. Relatively few myelinated nerve fibers were present through the three-dimensional 1-month-old spinal cord lesion.

4. Discussion

We believe our double labeling technique images the histopathology of the chronic spinal cord lesion in a way not possible by inspecting serial 2D sections or by other three-dimensional imaging methods. Being able to 3D surface reconstruct alternate groups of transverse sections increases the number of histopathological events to be visualized from a single spinal cord. By interpolating the space between the groups of differently stained sections, we were able to successfully reconstruct two highly accurate 3D visualizations of the same injured spinal segment revealing

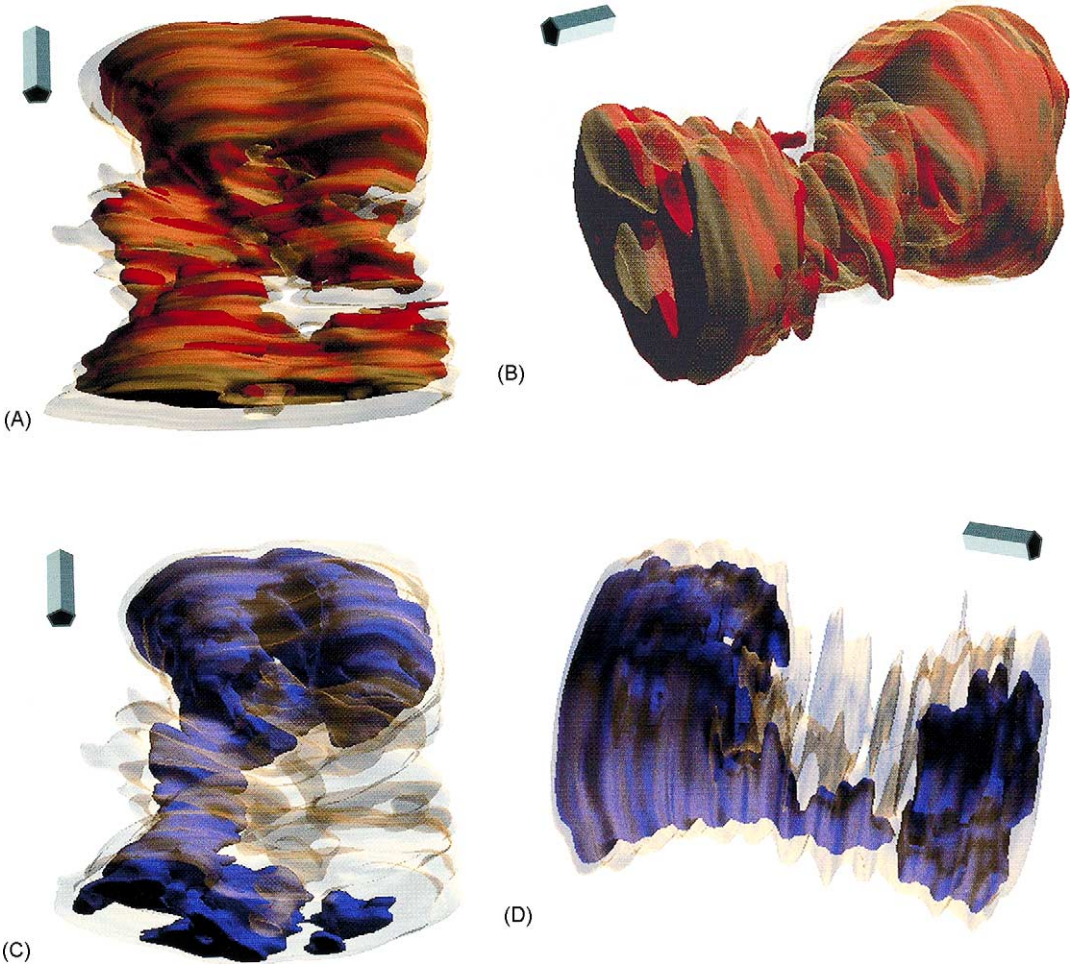

Fig. 5. Comparison of MT and LFB 3D reconstructions to the full 3D reconstruction. These images illustrate the differences of the labeled features of the MT and LFB 3D reconstructions compared to the entire reconstructed spinal segment. In (A) and (B), the MT 3D reconstruction shown in red is merged with the full 3D reconstruction comprised of both MT and LFB consecutive histological sections (transparent gold). The dorsal view in (A) and lateral view in (B) show a strong correspondence between 3D reconstructions, particularly at the uninjured distal ends of the spinal segment. (C) and (D) show the LFB reconstruction in blue with the full 3D reconstruction in transparent gold. (C) The dorsal aspect of these two reconstructions show the relatively small sparing of myelinated nerve fibers across the site of injury. (D) The lateral view of the combined LFB and full reconstructions demonstrate that myelinated fibers are found in the ventrolateral white matter tracts only on one side of the spinal cord. There was more substantial LFB staining at the distal ends of the spinal segment (C) and (D).

different pathological features. These 3D reconstructions were 50% interpolated, which is better than the sampling rate typically used in other 3D reconstructions in the literature with ranges from 67 to 98% interpolation or one slice out of three being 3D reconstructed to one slice out of 25 (Beattie et al., 1997; Bresnahan et al., 1991; Chawla et al., 1981; Chimento et al., 1994; Liss, 1995).

The double labeling technique was well suited for 3D reconstructing the injured spinal cord segment from transverse sections. We believe that the shape of the histological sections must be fairly uniform or the interpolated series of sections would not be consistent with the shape of the actual sections that were being replaced. As the morphology of a normal segment of spinal cord corresponds to an elliptical cylinder, transverse sections remain very consistent in size and shape (Blight, 1991). Even in the compressed spinal cord where it forms an hour-glass shape with the damaged area located at the narrowest point, cross-sections gradually change size. It is likely that the double labeling technique could not be reliably performed using sections that vary greatly in shape, like longitudinal sections of spinal cord or sections from irregular tissues. Interpolation of absent sections that vary greatly in size and shape would cause significant inconsistencies to the morphology of the 3D reconstruction.

The isocontouring program we employed has significantly hastened 3D reconstruction by producing three-dimensional surfaces around discrete areas of interest that have the same pixel value. Thus, 3D reconstruction by isocontouring does not require much human intervention. In addition, this technology allows reconstructions to be quantified. Object counting and length measurements of reconstructions and their

relationship to other structures of interest have frequently been made (Hashimoto and Kimura, 1988; Hounnou et al., 2003; Salisbury, 1994). Our laboratory has shown that 3D reconstructions of spinal cord pathological structures, such as cysts, lesion, and nervous tissue sparing can be accurately measured for volume and surface area (Duerstock et al., 2000, 2003; Moriarty et al., 1998).

We plan to apply other cellular and tissue markers for use with this double labeling 3D reconstruction technique in order to define other anatomical and pathological features. We hope that by combining different histological markers other inflammatory and cytolytic events can be imaged at specific time points after spinal cord injury. Understanding the interplay of these cascades would help better understand the complex pathogenesis that occurs during secondary injury.

Acknowledgements

I wish to thank Dr. Richard B. Borgens, Director of the Center for Paralysis Research, for his support of this project. Dr. Chandrajit Bajaj, Director of the Center for Computational Visualization at the University of Texas at Austin, generously provided the isocontouring program for 3D reconstruction. I greatly appreciate Debbie Bohnert and Carie Brackenbury for their technical assistance and Stacey Folyer for manuscript preparation. Financial support was provided by AASERT—DAAH04-93-G-101 to R.B.B. and NIH 1R01NS/HD39288-01A1 to R.B.B. and by funds provided to the Center for Paralysis Research by the State of Indiana. Intel personal computers used in this study were graciously donated by Intel® Corporation.

References

Bajaj CL, Pascucci V, Schikore DR. The contour spectrum. In: Proceedings of the IEEE Visualization'97 Conference. ACM Press; 1997.

Balentine JD. Pathology of experimental spinal cord trauma. I. The necrotic lesion as a function of vascular injury. Lab Invest 1978;39(3):236–53.

Beattie MS, Bresnahan JC, Komon J, Tovar CA, Van Meter M, Anderson DK, Faden AI, Hsu CY, Noble LJ, Salzman S, Young W. Endogenous repair after spinal cord contusion injuries in the rat. Exp Neurol 1997;148:453–63.

Blight AR. Morphometric analysis of a model of spinal cord injury in guinea pigs, with behavioral evidence of delayed secondary pathology. J Neurol Sci 1991;103:156–71.

Bresnahan JC, Beattie MS, Stokes BT, Conway KM. Three-dimensional computer-assisted analysis of graded contusion lesions in the spinal cord of the rat. J Neurotrauma 1991;8(91):91–101.

Chawla SD, Glass L, Proctor JW. Three-dimensional reconstruction of disseminated cancer modules. Cancer Biochem Biophys 1981;5:153–61.

Chimento TC, Doshay DG, Ross MD. Compartmental modeling of rat macular primary afferents from three-dimensional reconstructions of transmission electron micrographs of serial sections. J Neurophysiol 1994;71(5):1883–96.

Duerstock BS, Bajaj CL, Borgens RB. A comparative study of the quantitative accuracy of three-dimensional reconstructions of spinal cord from serial histological sections. J Microsc (Oxford) 2003;210(Pt 2):138–48.

Duerstock BS, Bajaj CL, Pascucci V, Schikore D, Lin K, Borgens RB. Advances in three-dimensional reconstruction of the experimental spinal cord injury. Comput Med Imag Graph 2000;24(6):389–406.

Duerstock BS, Borgens RB. Three-dimentional morphometry of spinal cord injury follow polyethylene glycol treatment. J Exp Biol 2002;205:13–24.

Halliday GM, Cullen K, Cairns MJ. Quantitation and three-dimensional reconstruction of Ch4 nucleus in the human basal forebrain. Synapse 1993;15:1–15.

Hashimoto S, Kimura RS. Computer-aided three-dimensional reconstruction and morphometry of the outer hair cells of the Guinea Pig cochlea. Acta Otolaryngol (Stockholm) 1988;105:64–74.

Hounnou G-M, Uhl J-F, Plaisant O, Delmas V. Morphometry by computerized three-dimensional recontruction of the hypogastric plexus of a human fetus. Surg Radiol Anat 2003;25:21–31.

Liss AG. Computer-assisted method for simultaneous three-dimensional reconstruction of highly magnified nerve endings and low-magnification contours of the spinal cord. J Microsc (Oxford) 1995;178(Pt 2):160–4.

Moriarty LJ, Duerstock BS, Bajaj CL, Lin K, Borgens RB. Two- and three-dimensional computer graphic evaluation of the subacute spinal cord injury. J Neurol Sci 1998;155(2):121–37.

Roesch S, Mailly P, Deniau JM, Maurin Y. Computer assisted three-dimensional reconstruction of brain regions from serial section digitized images: application to the organization of striato-nigral relationships in the rat. J Neurosci Methods 1996;69:197–204.

Salisbury JR. Three-dimensional reconstruction in microscopical morphology. Histol Histopathol 1994;9:773–80.

Tator CH, Fehlings MG. Review of the secondary injury theory of acute spinal cord trauma with emphasis on vascular mechanisms. J Neurosurg 1991;75:15–26.

Young W, Huang PP, Kume-Kick J. Cellular, ionic, and biomolecular mechanisms of the injury process. In: Benzel EC, Tator CH, editors. Contemporary Management of Spinal Cord Injury, vol. 27–42. AANS Publications Committee; 1995.